Modelling pyrolysis process for PP and HDPE inside thermogravimetric analyzer coupled with differential scanning calorimeter

Shawki Mazloum, Youssef Aboumsallem, Sary Awad, Nadine Allam, Khaled Loubar

Version of Record: https://www.sciencedirect.com/science/article/pii/S0017931021005718
Manuscript_e3d867f83ab85eb79d8613826d296328

Modelling pyrolysis process for PP and HDPE inside thermogravimetric analyzer coupled with differential scanning calorimeter

Shawki MAZLOUM[1,2], Youssef ABOUMSALLEM[2], Sary AWAD[1*], Nadine ALLAM[2], Khaled LOUBAR[1]

[1] *GEPEA, UMR 6144, Energy Systems and Environment Department, IMT Atlantique, 04 rue Alfred Kastler, CS 20722, 44307 Nantes Cedex 3, France.*

[2] *Lebanese International University, Beirut, Lebanon*

**Corresponding author:* Sary AWAD*, sary.awad@gmail.com*

Abstract

Plastic pyrolysis is widely studied and implemented at lab-scale but rarely modelled numerically. For the sake of designing efficient industrial reactors, modelling plastic pyrolysis process at particle scale could be a prerequisite. Therefore, the aim of this work is to model the whole plastic pyrolysis process, on particle scale, for polypropylene (PP) and high density polyethylene (HDPE) inside a thermogravimetric analyzer coupled with differential scanning calorimeter (TGA-DSC). First, the kinetic triplet for PP and HDPE pyrolysis, at heating rates 4-10 °C/min, are determined according to the isoconversional methods. Secondly, the kinetic triplets are used along with the appropriate conditions to model and simulate the pyrolysis process for PP and HDPE in TG analyzer, using finite element method. The melting sub-process is modelled using the modified apparent heat capacity method, which resulted in a relative error below 10% between the simulated and measured heat flow. Furthermore, the cracking model describes perfectly PP and HDPE cracking, where the average relative error among all calculated and experimental conversions didn't exceed 5%. Furthermore, the heat flow inside the TGA-DSC crucible was modelled and the average error was reduced to less than 8% by dividing the cracking phenomena into a "latent" and an apparent process.

Keywords: TGA-DSC; Plastic Pyrolysis; Modelling; Finite Elements; Kinetics;

1. Introduction

Nowadays, plastics became the most utilized material in daily life activities and industry. Plastic production started in 1950s and increased enormously each year to reach nearly 360 million tons in 2018, and the rate is still increasing [1]. Post-consumer plastics turn into solid wastes at the end of its service life, which varies between one day and more than 50 years. Therefore, plastic wastes are generated in massive amounts every year, it reached 307 million tons worldwide in 2015 [2]. Where olefin materials i.e. polyethylene (PE) and polypropylene (PP) constitute 60 % of the annual plastic wastes produced worldwide. On the other hand, three main processes are used to treat plastic waste disposal: recycling, energy recovery, and landfilling. Whereas in Europe 2018, 29.1 million tons of plastic wastes are collected and treated as follow; 32.5% are recycled, 42.6% are energy recovered and 24.9% are landfilled [1]. And since plastics are non-degradable material, landfilling process is ineffective and pollutant treatment method, that should be reduced. Thus, recycling and recovery processes should be more employed [1]. In addition, fossil fuel reservoir diminishing dilemma is facing the coming generations; thus the pursue for alternative green renewable energy processes is required.

One of the efficient processes for plastic wastes management is plastic pyrolysis process: it converts plastic wastes into a wide range of hydrocarbons via thermal degradation of the long chain polymers at a given temperature and in absence of oxygen [3]. Plastic pyrolysis process is widely implemented and studied experimentally in lab-scale reactors, where many research papers investigated: pyrolysis kinetics, affecting parameters and characteristics of by-products [3-7]. On the other hand, it is rarely modelled and studied numerically. Moreover, simulation and numerical studies for lab-scale reactors help in upgrading and designing efficient reactors that can be employed in the industrial sector, by optimizing the operating conditions and the geometry of the reactor.

Bockhorn et al. [8] and Navarro et al. [9] analytically modelled pyrolysis process for plastic particles inside a thermogravimetric analyser, using a zero-dimension model. They applied different values for the global heat transfer coefficient depending on the type of the reactor: 100 $W.m^{-2}.K^{-1}$ to 1000 $W.m^{-2}.K^{-1}$ for fluidized-bed reactors, while a value of 10 $W.m^{-2}.K^{-1}$ for fixed bed reactors [9]. On the other hand, Jin et al. [10] modelled pyrolysis process for a thin film flow for polyethylene (PE), polypropylene (PP), and polystyrene (PS) inside a vertical falling film reactor, using the volume of fraction (VOF) model [11-13]. Furthermore, they

deduced that the apparent heat transfer coefficient for pyrolyzed plastic in the falling film reactor is greater than that in the rotary kiln reactor: 4000 and 1000 $W.m^{-2}.K^{-1}$ respectively [14]. Moreover, Csukas et al. [15] modelled plastic pyrolysis in a continuous tubular reactor using Direct Computer Mapping (DCM) i.e. C++ algorithm with a graphical user interface, but without mentioning the global heat transfer coefficient used. In addition, most of the studies nominate the one-step model to describe plastic pyrolysis [16,17]. Whereas, Ding et al. [16] modelled pyrolysis process for plastic particles inside a fluidized bed reactor using one-step model; the results were compatible and validated with the experimental data. Nevertheless, modelling and simulating plastic pyrolysis process based on the solution of governing equations within the bulk of material, using finite elements approach, are still rarely found in literature.

Furthermore, determining of the kinetics of pyrolysis is the first step required to model and simulate any pyrolysis process. And for a thermal decomposition process, the thermogravimetric techniques are the best way to evaluate the kinetic parameters. Several researchers studied the thermal degradation kinetics of plastic waste at low heating rates (i.e. below 50 °C/min), and they presumed that the pyrolysis reaction could be identified by the *n*th order model, i.e. the plastic pyrolysis reaction mechanism is assumed to follow the function: $f(x) = (1 - x)^n$, where x is the conversion and n is the power indicating the reaction order [18-20]. Consequently, other attempts have been made to identify the reaction model for polyethylene and polypropylene by several similar-like methods: Reduced-time-plots method, Criado's method, and Coats-Redfern method [4, 5, 21, 22]. Additionally, the thermogravimetric analysis (TGA) is used along with the isoconversional methods to study the pyrolysis kinetics for the most significant components of the municipal plastic wastes, polyethylene and polypropylene, and to determine the activation energy and the frequency factor [23, 24]. Therefore, in this work the Criado's method will be used along with the TGA data to find the best reaction models that describe the pyrolysis process for high density polyethylene (HDPE) and polypropylene. In addition, the activation energy and the frequency factor will be evaluated according to the literature's three standard isoconversion methods: Friedman (FR) method, Kissinger-Akahira-Sunose method (KAS), and Flynn-Wall-Ozawa method (FWO).

Moreover, knowing the fact that pyrolysis process includes different sub-processes; heating, melting and cracking, it is necessary to model the melting process prior to the cracking phase. But on the other hand, modelling and simulating melting process for plastics is rarely found in

literature, where there is no clear model that simulates and describes the melting process for bulk amounts of plastics. Whereas, many research papers investigate modelling and simulating melting process for other materials, especially phase change material (PCM). A numerical and experimental study was done by Madruga et al. [25] to investigate the melting phenomena for tetracosane paraffin inside a cubic enclosure: it was heated from 40 °C, as an initial temperature, to around 80 °C. The cubic enclosure was heated from the bottom by a constant wall temperature of 80 °C. The apparent heat capacity method (AHCM) was used to model the melting process for tetracosane paraffin, where they used a linear phase change function to model the melting process. Moreover, the experimental and numerical results were in a good agreement. Furthermore, Murray et al. [26] and Samara et al. [27] have modelled the melting process for other phase change materials: octadecane and RT25, using the AHCM. The phase change materials were heated by a uniform heat flux from the side of a rectangular enclosure from the ambient temperature 27 °C to the desired temperature 40 °C passing through the melting temperature (T_m = 30 °C). They used a piecewise impulse function for the heat capacity of the materials to model the melting phenomena. On the other hand, Salvi et al. [28] modelled the phase change process for a carboxymethyl cellulose solution by a predefined Gaussian distribution function (δ). This Gaussian function (δ) was multiplied by the material's latent heat of melting to model the heat absorption or sink during the phase change process: the numerical and experimental results were in good agreement with an average coefficient of determination R^2 = 0.91. As a result, the modified AHCM with a smooth distributed Heaviside function will be used in the present work to model the melting process for PP and HDPE prior the cracking phenomena.

Finally, as it is previously mentioned that there is a gap in modelling and simulating plastic pyrolysis process using finite element approach. Thus, the objective of this paper is to model and simulate the whole plastic pyrolysis process, on particle size scale, for PP and HDPE inside a thermogravimetric analyzer coupled with differential scanning calorimeter (TGA-DSC). This work will be, later on, a prerequisite for modelling and validating plastic pyrolysis process in lab-scale reactors (semi-batch or continuous reactors) for the sake of upgrading and designing efficient industrial reactors by numerical optimization.

The present work will be divided into the following steps: (1) modelling and validating melting and heating processes for PP and HDPE inside TGA-DSC by comparing the heat flow (absorbed energy by the material), (2) determining the pyrolysis kinetic parameters for PP and HDPE using the TGA experimental results, and (3) using the deduced pyrolysis

kinetic parameters to model and validate the cracking process for PP and HDPE inside TGA-DSC via heat flow comparison. Furthermore, modelling an interesting experimental phenomena, pre-cracking phenomena (latent cracking), which is deduced to be occurring before and along the mass loss cracking of the material.

2. Materials and methods

2.1. TGA-DSC experiments and procedure

SETSYS Evolution instrument is used to conduct simultaneous TG-DSC analysis for PP and HDPE pyrolysis at different heating rates. Where two aluminum crucibles (100 µL capacity), one for reference and one to hold sample, are heated by a graphite furnace that controls the temperature and the heating rate of the sample. Moreover, an electric microbalance measures the mass loss of the sample over time (± 1 µg deviation).

Four pyrolysis experiments are realised for PP and HDPE at different heating rates (4, 6, 8, and 10 °C/min), where each experiment is replicated. First, the pyrolyzed samples (weight varies between 16 and 19 mg) are sustained at isothermal state (25 °C) for 20 min. Second, the sample temperature is heated up to 500 °C at different constant heating rates (4, 6, 8, and 10 °C/min). Moreover, during the process, the system is purged using nitrogen gas (N_2) of 20 mL/min volumetric flow rate to prevent oxidation reaction and to carry on the by-product gases. Furthermore, the sample temperature (°C), the mass (mg), and the heat flow (that is absorbed by the sample material) are all recorded for further analysis, as shown in Figs. 1 and 2 below for the HDPE.

As it is noticed from the above figures, the increase of heating rate (β) slightly increases the peak temperatures and the enthalpies for melting and cracking processes. Furthermore, the heat flow for HDPE (Fig. 2) is almost constant between the melting and cracking (from 200 to 360 °C). Thus, the heat capacity for HDPE is constant in this region and equals to 2500 J/kg.K in contrast to PP heat capacity, which increases from 2200 to 2500 J/kg.K as temperature rises from 200 to 300 °C. Moreover, the heat capacities for PP and HDPE increase from 1800 to 2200 J/kg.K and from 1800 to 2500 J/kg.K, respectively, as the temperature increases from 80 to 200 °C during the melting process. Furthermore, the melting enthalpies ΔH_m and the cracking enthalpies ΔH_c, listed in Table 1, are determined by integrating the experimental heat flow (HF), according to the tangential method, between the onset and offset temperatures of the corresponding processes (melting or cracking). These values are also checked and found in literature supported by different references [10, 29-31].

2.2. Raw materials

Virgin granules of polypropylene, with 2–3 mm as particle size, and post-consumed high density polyethylene, chopped into small flakes of dimension 4 × 2 mm, are used to conduct the pyrolysis experiments using TG-DSC analyzer. The thermal conductivities for PP and HDPE are assumed to increase linearly from 0.1 to 0.12 W/K.m and from 0.42 to 0.45 W/K.m, respectively, as the material changes phase from solid to molten state (25 to 200 °C). The thermo-physical properties for these materials and for the aluminum crucible are shown in Table 2 [10, 29-31].

2.3.General methodology adopted for simulation

First of all, the kinetic parameters for PP and HDPE pyrolysis are determined using the experimental TGA data. Then these parameters are implemented into numerical simulation using COMSOL Multiphysics with appropriate equations and boundary conditions to model the pyrolysis process for PP and HDPE inside the thermogravimetric analyzer. Finally, the calculated power absorbed by the pyrolyzed material over time is compared to the experimental heat flow recorded by the DSC. After that, the relative error is calculated among the experimental and simulated results by Eq. (1) for further validation.

$$Rel\_error_{HF} = \frac{HF_{exp} - HF_{sim}}{HF_{exp}} * 100 \quad (1)$$

Where HF_{exp} and HF_{sim} are respectively the experimental and the simulated heat flow absorbed by the pyrolyzed material over time during the whole pyrolysis process.

The TGA/DSC analyzer includes two aluminum crucibles; one contains the sample material (plastic) as shown in Fig. 3-(a), and the other is empty (reference crucible). These two crucibles are heated from the sides via radiation by, a hollow cylindrical shape, programmable electrical furnace, where the crucibles are located in the center. In addition, the aluminum sample crucible (100 µL volume and 4 mm diameter) with plastic material inside is drawn as 2D-axisymetric with the exact dimensions as measured from the instrument, shown in Fig. 3-(b). COMSOL Multiphysics is used to carry out the modelling and the numerical studies, where a linear temperature, $T_{exp}(t)$, depending on the experimental constant heating rate β (°C/min), is set as the heat boundary condition on the side wall of the sample crucible, as shown by Fig. 3-(b).

Moreover, the solution was converged using an extremely fine mesh of element size that doesn't exceed 0.09 mm, where further decrease in the element size didn't change the solution. Whereas for the skewness and condition number mesh characteristics, the values of minimum and average element qualities are 0.6 and 0.9, respectively, for 2000 triangular element as shown by Fig. 3-(c). In addition, a direct solver (PARDISO algorithm: Parallel Direct Solver) is used to solve the linearized system at each iteration set by the Newton's Method (Newton-Raphson Method) with an automatic damping factor, which is used to solve the non-linear problems.

Consequently, the time stepping method follows the BDF algorithm (Backward Differentiation Formula), which is an implicit solver that uses backward differentiation formulas with order of accuracy varying from one (also known as the backward Euler method) to five, whereas the maximum time step is 0.2 s. Finally, an absolute tolerance equals to 0.0001 is used as the termination technique for the solver.

Furthermore, the heat transfer module, governed by the energy equation, is combined with melting and cracking models to simulate the whole pyrolysis process. Finally, the molten plastic inside the crucible is assumed to be a stationary fluid because of the small volume (2 mm radius and 2 mm height) and the high viscosity (more than 1000 Pa.s) of the molten plastic, especially at low shear rates [32].

2.4. Pyrolysis kinetics modeling

Pyrolysis process is the sum of unknown large number of chemical reactions that occur. The long chain molecules of plastics decompose and break randomly to form light chain hydrocarbons or radicals. Even more, these primary by-products may further crack to form other lighter chains or recombine to form longer ones. Therefore, plastic pyrolysis is the sum of complex chemical reactions that can't be modelled or tracked according to the stoichiometric coefficients of the occurring chemical reactions. On the other hand, plastic pyrolysis process can be modelled as single step reaction that overcomes all the complexity of the existing reactions. Many research papers investigated and used the one step reaction to model the pyrolysis process for PP, HDPE, and other types of plastics [18-22]. The kinetic equation represented by Eq. (2) describes the rate of conversion dx/dt (s^{-1}) of the one step pyrolysis reaction model. Where, K(T) (s^{-1}) represents the kinetic constant of the reaction and f(x) presents the reaction model of the whole pyrolysis reaction [33].

$$\frac{dx}{dt} = K(T)\, f(x) \tag{2}$$

The conversion x ($0 < x < 1$) is described by Eq. (3), where m_0 (mg) is the initial mass, m_t is the residual mass (mg) at time t (s), and m_∞ is the residual mass (mg) at the end of the process.

$$x = \frac{m_0 - m_t}{m_0 - m_\infty} \tag{3}$$

Furthermore, K(T) is a function depending on temperature, and is also represented by the Arrhenius equation, Eq. (4), where E (J/mol) is the activation energy, A is the pre-exponential component called the frequency factor, and R is the universal gas constant (8.314 J/mol.K).

$$K(T) = A\, exp\left(\frac{-E}{R\,T}\right) \tag{4}$$

Moreover, f(x) is selected from the most common reaction mechanisms shown in Table 3 [4], where g(x) is the integrated form of the reciprocal of the reaction model f(x), with respect to the conversion dx, Eq. (5):

$$g(x) = \int_0^x \frac{dx}{f(x)} \tag{5}$$

The aim here is to determine the kinetic triplet: E, A, and $f(x)$. First of all, the reaction model f(x) is determined by the Criado's method, Eq. (6). Which is a graphical curve fitting method that compares all the theoretical reaction models f(x), presented in Table 3 and normalized by Eq. (7), with the experimental function $f_{experimental}$, Eq. (8), for each heating rate [34].

$$\frac{z(x)}{z(0.5)} = \frac{f(x)g(x)}{f(0.5)g(0.5)} = \left(\frac{T_x^2}{T_{0.5}^2}\right)\frac{(dx/dt)_x}{(dx/dt)_{0.5}} \tag{6}$$

$$f_{theoretical} = \frac{f(x)g(x)}{f(0.5)g(0.5)} \tag{7}$$

$$f_{experimental} = \left(\frac{T_x^2}{T_{0.5}^2}\right)\frac{(dx/dt)_x}{(dx/dt)_{0.5}} \tag{8}$$

where $T_{0.5}$ and $(dx/dt)_{0.5}$ represent the temperature and conversion rate at $x = 0.5$. The purpose of dividing by 50% condition is to normalize the $z(x)$.

Then the coefficient of determination (R^2) is calculated between the experimental curves and the theoretical curves for each heating rate (β). Finally, the models that have the highest regression coefficient (R^2) are chosen to be the best fitting reaction models.

The second step in pyrolysis kinetic study is to find the activation energy E (J/mol), so the isoconversional concept must be introduced. The kinetic equation or so-called Friedman equation, Eq. (2), is manipulated by applying the logarithmic function on both sides and differentiating by 1/T at a constant conversion x to give Eq. (9) [35].

$$\left[\frac{\partial\, ln(dx/dt)}{\partial T^{-1}}\right]_x = -\frac{E}{R} \tag{9}$$

Thus, from interpreting Eq. (9) the isoconversional concept is illustrated, where it states that the rate of conversion (dx/dt) at a constant conversion (x) is only function of temperature. Therefore, the activation energy E (J/mol) is the same at each constant conversion x for different temperatures at different heating rates. Thus different isoconversional methods are invented to calculate the activation energy at every conversion x using the TGA experimental results (x, dx/dt, $1/T$, and β). The Friedman method, expressed by Eq. (10), is the first differential isoconversional method, where the activation energy is determined from the slope ($-E\ /\ R$) of the linear fitting straight lines of plotting $\ln(dx/dt)$ with respect to $1/T$ for different heating rates (i.e. different temperatures) at a constant conversion x. Moreover, the coefficient of determination (R^2) is calculated between the linear fitting straight lines and the experimental data or points.

$$\ln\left(\frac{dx}{dt}\right) = \ln[A\, f(x)] - \frac{E}{R\, T} \tag{10}$$

For the sake of methods comparison, two other integral isoconversional methods will be used to evaluate the activation energy [10-15]. The two methods are: Kissinger-Akahira-Sunose (KAS), Eq. (11), and Flynn-Wall-Ozawa (FWO), Eq. (12).

$$\ln\left(\frac{\beta}{T^2}\right) = \ln\left[\frac{A\, R}{E\, g(x)}\right] - \frac{E}{R\, T} \tag{11}$$

$$\ln \beta = \ln\left[\frac{A\, E}{R\, g(x)}\right] - 5.331 - 1.052\, \frac{E}{R\, T} \tag{12}$$

Same methodology is followed to determine the activation energy by KAS and FWO method, where the corresponding slopes are determined from the linear fitting straight lines for

plotting $\ln(\beta/T^2)$ or $\ln\beta$ with respect to $1/T$ for different heating rates (i.e. different temperatures) at a constant conversion .

Finally, the third kinetic parameter A (1/s) is determined from each isoconversional equation, Eqs. (10-12), by calculating the intercept values for the fitting straight lines and by using the deduced previous kinetic parameters E and f(x). After finding the kinetic triplet for the pyrolysis process, the final step is to calculate the theoretical conversion (by solving the kinetic equation Eq. (2)) and to compare the results with the experimental results for further validation.

2.5. Apparent heat capacity method for phase change modelling

After a literature investigation, there is no specific method or equation to model plastic melting phenomena. Whereas, there exists a well-known method that models in general the phase change phenomena for any material, including the melting process. This method is called the apparent heat capacity method (AHCM) and it is used to model the melting process for many different phase change materials (PCM) [25-28]. The main concept of this method is to gradually add the latent heat to the heat capacity of the material directly in the energy equation during the melting or phase change process. Madruga et al. [25] used the AHCM method to study numerically the melting process for tetracosane paraffin within a cubic enclosure using a linear conversion function f_l. Moreover, to model the heat sink during the melting process, the derivative of f_l with respect to time (df_l/dt) is multiplied by the density and the melting latent heat of the material. Eqs. (13) and (14) show the conversion function f_l and the heat sink Q_s.

$$\boldsymbol{f_l = \begin{cases} 0, & T \le T_s \\ 1, & T \ge T_l \\ (T - T_s)/(T_l - T_s), & T_s < T < T_L \end{cases}} \quad \textbf{(13)}$$

$$Q_s = \rho \Delta H_m \frac{df_l}{dt} \quad (14)$$

T_s (°C) and T_l (°C) are respectively the temperatures of the beginning and end of melting process. Whereas, ΔH_m (kJ/kg) is the latent melting heat and ρ (kg/m^3) is the density of the paraffin.

Salvi et al. [28] and Samara et al. [27] also implemented the apparent heat capacity method in their work using a smoothed distributed function called the Gaussian distribution function δ, described by Eq. (15).

$$\boldsymbol{\delta = \frac{exp(-(T-T_{pc})^2/(\Delta T/2)^2)}{(\Delta T/2)\sqrt{\pi}}} \quad \textbf{(15)}$$

where T_{pc} (°C) is the phase change temperature and ΔT (°C) is the phase change temperature interval. But in this method, the phase change function (conversion) cannot be displayed or modified. In addition, simulation may take long time or diverge because of the discontinuity that occurs by the activation of the Gaussian function.

A more advanced form of AHCM methods is the modified apparent heat capacity method (AHCM) used and built-in COMSOL Multiphysics. In this method, there exists a continuous smoothed Heaviside function called θ_1, distributed along ΔT and having T_{pc} as a median temperature, that can be modified or displayed for any point in the simulated domain (molten fluid) [36]. This function is differentiated with respect to temperature and multiplied by the phase change enthalpy ΔH_{pc} (melting) then added to the average heat capacity $C_{p,eq}$ of the material, as shown in Eqs. (16) and (17).

$$\boldsymbol{C_{p,app} = C_{p,eq} + C_L(T)} \quad \textbf{(16)}$$

$$C_{p,app} = \frac{1}{\rho_{eq}}\left(\theta_1 \rho_{ph1} C_{p,ph1} + \theta_2 \rho_{ph2} C_{p,ph2}\right) + \Delta H_{pc}\frac{d\theta_1}{dT} \quad (17)$$

Where $C_L(T)$ is the latent heat distribution over the melting interval ΔT, ρ_{eq} is the equivalent density, θ_1 is the phase indicator for phase 1 (*ph1*), $\theta_2 = 1 - \theta_1$ is the phase indicator for phase 2 (*ph2*), ρ_{ph1} is the density of phase 1, and $C_{p,ph2}$ is specific heat capacity for phase 2. Moreover, the equivalent density and thermal conductivity are shown in Eqs. (18) and Eq. (19):

$$\boldsymbol{\rho_{eq} = \theta_1 \rho_{ph1} + \theta_2 \rho_{ph2}} \quad \textbf{(18)}$$

$$k_{eq} = \theta_1 k_{ph1} + \theta_2 k_{ph2} \quad (19)$$

Therefore, the advanced AHCM that is found in COMSOL Multiphysics will be used to model the melting phenomena for PP and HDPE inside the TGA-DSC as a sub-step of the pyrolysis process.

2.6. Governing equations and boundary conditions for simulation

After determining the kinetic parameters for PP and HDPE pyrolysis and finding the melting model for plastics, these models will be implemented into numerical simulation with the appropriate governing equations and boundary conditions to model the pyrolysis process for

PP and HDPE inside TGA-DSC. The heat conduction equation, Eq. (20), is used to model heat transfer within the plastic sample and the aluminum crucible [32,37].

$$\rho C_p \frac{\partial T}{\partial t} = Q + \vec{\nabla} . k\vec{\nabla}T \quad (20)$$

where ρ is the density (kg/m^3), C_p is the specific heat capacity (J/(kg.K)), Q is the volumetric heat source or sink term (W/m^3), $\vec{\nabla}$ is the gradient operator (∂_x, ∂_y, ∂_z), k is the thermal conductivity (W/(K.m)), and T is temperature (°C). Moreover, the melting model is coupled with the heat conduction equation by replacing the heat capacity C_p and thermal conductivity k in Eq. (20) with the apparent heat capacity $C_{p,app}$ and the average thermal conductivity k_{eq} described respectively in Eqs. (17) and (19). The solid and molten densities, for PP or HDPE, are taken as constant average values as shown in Table 2, since the volume of the material in the simulation doesn't change. Additionally, to model the cracking part, the heat sink term in Eq. (20) is replaced by $Q_s = \rho \Delta H_c \, dx/dt$, where ΔH_c is the cracking enthalpy given in Table 1 and dx/dt is the rate of conversion described by the kinetic equation Eq. (2). Also, to model the mass loss during the cracking part and since the volume of plastic is fixed in our simulation, a variable density $\rho(T)$ function of temperature is used. This density $\rho(T)$, shown in Fig. 4, is determined by dividing the experimental mass of the sample over time, shown in Fig. 1, by the fixed volume of the pyrolyzed material.

Regarding the boundary conditions, the crucible is surrounded by the electrical heater and heated from the side wall mainly by radiation mode. In addition, the temperature of the crucible is controlled by adjusting the heating rate for each experiment.

The crucible filled with the plastic material is modelled as 2D-axisymetric domain. In addition, a theoretical uniform profile temperature corresponding to the experimental constant heating rate for each experiment (4 to 10 °C/min) is taken as a heat boundary condition at the side wall of the crucible. Therefore, the plastic material and the crucible are heated linearly by a constant heating rate from the ambient temperature (25 °C) to 500 °C.

3. Results and discussion

3.1. Pyrolysis kinetics results for PP and HDPE

First the Criado's method, Eq. (6), is used to determine the best fitting reaction models for PP and HDPE that have the highest coefficient of determination R^2. For example, Figs. 5 and 6 illustrate the results for PP at different heating rates. Moreover, the best reaction models, that

are deduced, with the highest average coefficient of determination for PP and HDPE pyrolysis are as follow: A2 (R^2 = 0.97) and R3 (R^2 = 0.95) for PP and A2 (R^2 = 0.92) for HDPE. On the other hand, it is commonly found in literature that the reaction models for PP and HDPE are contracting sphere (R3) and contracting cylinder (R2), respectively, at relatively high heating rates above (10 °C/min) [4-5]. Moreover, in some studies it is found that the reaction model A2 represents the pyrolysis process for PP at low heating rates (below 10 °C/min) [21-22]. Furthermore, the difference in the reaction model between the deduced results (A2) and results found in literature (R3) can be due to the low heating rates adopted in the present work.

The second step is determining the activation energy E (J/mol) for PP and HDPE pyrolysis according to the three isoconversional methods; FR, KAS, and FWO. Fig. 7 shows the plot of the linear fitting of the experimental data for HDPE pyrolysis according to KAS method, where the value of the activation energy is evaluated from the slopes of these fitting straight lines at each conversion x. The results of the activation energy function of conversion for HDPE pyrolysis, according to all three methods, are illustrated in Fig. 8. As it is noticed, KAS and FWO methods gave approximately the same results with less variation function of conversion compared to FR method. Moreover, the determined values of the activation energies for PP and HDPE are within the ranges found in literature, 190 to 230 kJ/mol and 230 to 270 kJ/mol respectively [18-23]. Finally, the pre-exponential factor A (1/s) is determined using the deduced activation energy and reaction model, where Table 4 below summarizes all the deduced kinetic parameters for PP and HDPE (for heating rates from 4 to 10 °C/min).

Now the deduced average kinetic parameters are used to calculate the theoretical conversion by solving the kinetic equation, Eq. (2). This equation is solved by an iterative method to find the theoretical conversion x. After that, the theoretical conversions, according to the isoconversional methods and the selected kinetic models, are plotted and compared with experimental conversions to choose the best kinetic parameters (Table 5) based on the lowest average relative error. As a result, the Avarami-Erofe'ye (A2) reaction model with the activation energy and the frequency factor determined by either KAS or FWO methods are the best kinetic parameters to model pyrolysis process for PP and HDPE at low heating rates (below 10 °C/min). Moreover, the determined values of the activation energies for PP and HDPE are found to be within the ranges found in literature [18-23]. On the other hand, the deduced pre-exponential values differ from the values that are found in literature because the

deduced reaction models are different. Furthermore, Figs. 9 and 10 show the theoretical and experimental conversions for PP and HDPE pyrolysis according to the best fitting deduced kinetic parameters, where an average relative error between the results that didn't exceed 6 %.

3.2. Modelling and validating pyrolysis process for PP and HDPE inside TGA-DSC crucible

After finding the best kinetic parameters that model the pyrolysis process, the next step is to use these parameters in modelling and simulating PP and HDPE pyrolysis process inside TGA-DSC. Moreover, the AHCM is used in the simulation to model the melting phase before the pyrolysis process. All the appropriate equations, boundary conditions, and material properties, presented in sections 2 and 3, are applied and implemented into the simulations. As a result, Figs. 11 and 12 show the experimental and the simulated results, respectively for conversion and heat flow, for HDPE pyrolysis inside TGA-DSC, at 8 °C/min heating rate.

First of all, it is observed that the mass cracking model (TGA) is working perfectly well as shown in Fig. 11, where the average relative error among the simulated and experimental conversions is below 3 %. Moreover, Fig. 12 illustrates the DSC comparison results: the heat flow results seem to be alike, where they have the same response and trend over time.

Moreover, it is good to mention that the range of latent heat of fusion of HDPE found in literature is between 140 and 293 kJ/kg depending on the crystallinity of PE, ranging from 48 (140 kJ/kg) till 100 % (293 kJ/kg). However for LDPE the crystallinity is below 40 % (115 kJ/kg) [38 – 41]. In addition, the melting process is said to have two phases; First phase is the softening phase, between the start melting temperature and the onset temperature (for example between 98 and 119 °C for HDPE), where melting appears to be very slow in this part as shown in Fig. 13 below. However, the second part is the major part of melting which starts from the onset temperature till the end of melting. Whereas, this part constitutes more than 90 % of the melting phenomena and energy. Moreover and because of the symmetrical shape of the AHCM used and for the sake of simplicity, only the major part is modelled and calculated in this study as shown in Fig. 12, where the heat flow in the softening part is constant i.e. it is not modelled. Thus, the latent heat of fusion that is used in the simulation for HDPE is about 125 kJ/kg, which is calculated from the onset temperature as mentioned in section 2.1.

Therefore, if we add the energy of the softening part in Fig. 12 to the major latent energy of fusion used for HDPE, the result will be about 145 kJ/kg which is in the range of values that are found in literature.

Yet, a further improvement can be done to model this softening part, like by using AHCM to model this part or by using an exponential conversion function according to the Arrhenius law instead of the linear symmetrical conversion function used in this study. However, this is out of the scope of this study since it focuses on the cracking part. Also, about 10 % maximum error by modelling only the major part of the melting process is still an acceptable error.

Furthermore, the results (for HDPE and PP) are in a good agreement with the experimental data for the melting and heating phases (before the cracking phase) with an average relative error less than 7 %. In contrast to the cracking process, the error is relatively higher at this phase with an average value of 20 %.

Therefore, the model is said to be compatible to describe the cracking process for PP and HDPE that yield volatile products (TGA concept). Whereas, the DSC conception needs further apprehending and development to enhance the heat flow results at the cracking phase.

After interpreting carefully the TGA-DSC experimental results, it is noticed that a valuable amount of thermal energy is absorbed by the pyrolyzed material before mass loss occurs. The TGA-DSC heat flow results show that the absorbed heat increases starting from 360 °C till 425 °C (Figure 14) with a mass loss less than 0.08 % for the HDPE, and from 300 °C till 380 °C with a mass loss less than 0.06 % for the PP. Therefore, it is deduced that the cracking process starts before the mass loss occurs. In other words, the plastic molecules are decomposed into heavy liquid hydrocarbons that don't evaporate or escape the crucible. Thus pyrolysis could be decomposed roughly into two phases; during the first one plastic degrades into nonvolatile molecules, while during the second step, these latter are further decomposed to yield volatile hydrocarbons. Therefore, the first phase can be called 'latent cracking' or 'pre-cracking' and that should be modelled in order to approach the real case situation and to improve the simulated results.

By using the experimental heat flow results and the mass of the samples, the heat capacities for PP and HDPE are calculated just before the mass loss occurs (at 380 °C and 425 °C, respectively). Therefore, in order to model the latent cracking phenomena, the heat capacities for PP and HDPE are assumed to increase linearly from 2500 J/kg.K (at 300 °C for PP and at 360 °C for HDPE) to 3000 J/kg.K (at 380 °C) and to 3300 J/kg.K (at 425 °C). Moreover, to model this phenomenon during the second phase of cracking, the heat capacities are assumed to continue increasing linearly when the mass loss starts. The total heat flow, shown in Fig.

15, is decomposed into; sensible heat flow due to rise in temperature, latent cracking heat absorption, and apparent cracking heat absorption.

Fig. 16 illustrates the new results for HDPE pyrolysis after modelling the latent cracking phenomena. It is clearly noticed that the results are much enhanced, where the average relative error decreased to reach almost 6 %.

In addition, PP pyrolysis simulations are done using the same methodology with the appropriate heat capacity function, illustrated previously. As a result, all the simulated results for PP and HDPE pyrolysis processes are improved. Furthermore, the simulated results became very well compatible with the experimental ones with an average relative error below 8 % for all the heating rates, as shown in Fig. 17.

Further, it is deduced that the total cracking enthalpies ΔH_c for PP and HDPE, that are obtained from the DSC measurements and listed in Table 1 (in section 2.1. TGA-DSC experiments and procedure), are divided into two enthalpies in this model: the latent cracking enthalpy ΔH_{lc} and the apparent cracking enthalpy ΔH_{mc}, where it is revealed from the results, that the latent cracking enthalpies are almost half the value of the apparent cracking enthalpies for all PP and HDPE pyrolysis process simulations. Table 6 shows the constant values of the mass loss cracking enthalpies that are taken in these simulations and the deduced average latent cracking enthalpies from the numerical studies. In addition, it is obvious that the summation of the two preceding enthalpies is almost equal to the average total cracking enthalpies deduced from the experimental DSC measurements, as presented in Table 6.

5. Conclusions

An intensive kinetic study is performed for PP and HDPE pyrolysis, where the kinetic parameters for PP and HDPE are determined and compared with the results found in literature. First, the reaction models are determined using the Criado's method, which revealed that the Avarami-Erofe'ev (A2) model is the best reaction mechanism to model the pyrolysis process for PP and HDPE at low heating rates (below 10 °C/min). Moreover, the deduced values of the activation energies for PP (E = 220 kJ/mol) and HDPE (E = 264 kJ/mol) using the three isoconversional methods, FR, KAS, and FWO, fit within the ranges found in literature. In addition, kinetic parameters for PP and HDPE pyrolysis that gave the lowest average relative error are: $A = 4.15\times10^{15}$ (1/min) for PP, and $A = 8.3\times10^{17}$ (1/min) for HDPE. Besides, the average relative error between the theoretical conversions, according to

the best deduced kinetic parameters, and the experimental conversion for PP and HDPE pyrolysis at different heating rates (4 to 10 °C/min) didn't exceeds 6 %.

Furthermore, the deduced kinetic parameters are implemented along with the appropriate equations and boundary conditions into COMSOL Multiphysics software to model and simulate the whole pyrolysis process for PP and HDPE inside TGA-DSC. The apparent cracking model (TGA) worked perfectly well with an average relative error among all the simulated and experimental conversions for PP and HDPE pyrolysis less than 5 %. Moreover, the DSC comparison results, i.e. comparing the simulated heat flow results with the experimental ones, are enhanced by modelling the latent cracking phenomena that is occurring before and alongside apparent cracking. The average relative error decreased from 20 % to less than 8 % by modifying the heat capacity for PP and HDPE. Therefore it is noticed that the latent cracking enthalpy ΔH_{lc} is found to be almost half the value of the apparent cracking enthalpy ΔH_{mc} in all of the simulation results. Finally, the modified apparent heat capacity method (AHCM) revealed a high capability in modelling the melting processes for PP and HDPE, with an average relative error below 10 %. In addition, this complete modeling of plastic pyrolysis opens the way for simulating plastic pyrolysis in lab-scale reactors.

References

[1] Plastics – the Facts 2019, **An analysis of European plastics production; demand and waste data**, PlasticEurope, Association of Plastics Manufacturers, (2019).

[2] R. Geyer, J.R. Jambeck, K.L. Law, **Production, use, and fate of all plastics ever made**, Science Advances, 3 (2017).

[3] S.D.A. Sharuddin, F. Abnisa, W.M.A.Wan Daud, M.K. Aroua, **A review on pyrolysis of plastic wastes**, Energy Convers. Manage., 115 (2016), pp. 308-326.

[4] A. Aboulkas, K. El harfi, A. El Bouadili, **Thermal degradation behaviors of polyethylene and polypropylene. Part I: Pyrolysis kinetics and mechanisms**, Energy Convers. Manage., 51 (2010), pp. 1363-1369.

[5] F. Xu, B. Wang, D. Yang, J. Hao, Y. Tian, **Thermal degradation of typical plastics under high heating rate conditions by TG-FTIR: Pyrolysis behaviors and kinetic analysis**, Energy Convers. Manage., 171 (2018), pp. 1106-1115.

[6] C. Kassargy, S. Awad, G. Burnens, K. Kahine, M. Tazerout, **Experimental study of catalytic pyrolysis of polyethylene and polypropylene over USY zeolite and separation to gasoline and diesel-like fuels**, J. Anal. Appl. Pyrolysis, 127 (2017), pp. 31-37.

[7] Y. Zheng, L. Tao, X. Yang, Y. Huang, Z. Zheng, **Study of the thermal behavior, kinetics, and product characterization of biomass and low-density polyethylene co-pyrolysis by thermogravimetric analysis and pyrolysis-GC/MS**, J. Anal. Appl. Pyrolysis, 133 (2018), pp. 185-197.

[8] H. Bockhorn, A. Hornung, U. Hornung, et al., **Modelling of isothermal and dynamic pyrolysis of plastics considering non-homogeneous temperature distribution and detailed degradation mechanism**, J. Anal. Appl. Pyrolysis, 49 (1999), pp. 53-74.

[9] M.V. Navarro, J.D. Martínez, R. Murillo, et al., **Application of a particle model to pyrolysis. Comparison of different feedstock: Plastic, tire, coal and biomass**, Fuel Process. Technol., 103 (2012), pp. 1-8.

[10] Z. Jin, L. Yin, D. Chen, Y. Jia, B. Yu, **Heat transfer characteristics of molten plastics in a vertical falling film reactor**, Chin. J. Chem. Eng., 27 (2019), pp. 1015-1020.

[11] S. Liu, Y.L. Hao, **Numerical simulation on gas–liquid two-phase motion of falling film in vertical tube**, J. Therm. Sci. Technol., 7 (2008), pp. 5-10.

[12] E.G. Puckett, A.S. Almgren, J.B. Bell, et al., **A high-order projection method for tracking fluid interfaces in variable density incompressible flows**, J. Comput. Phys., 130 (1997), pp. 269-282.

[13] K. Yan, D.F. Che, **A coupled model for simulation of the gas–liquid two-phase flow with complex flow patterns**, Int. J. Multiphase Flow, 36 (2010), pp. 333-348.

[14] H. Wang, L.J. Yin, D.Z. Chen, et al., **Heat transfer characteristics of MSW and its typical components in rotary kiln at different pyrolysis stages**, J. Chem. Ind. Eng., 65 (2014), pp. 4716-4725.

[15] B. Csukas, M. Varga, N. Miskolczi, S. Balogh, A. Angyal, L. Bartha, **Simplified dynamic simulation model of plastic waste pyrolysis in laboratory and pilot scale tubular reactor**, Fuel Processing Technology, 106 (2013), pp. 186-200.

[16] K. Ding, Q. Xiong, Z. Zhong, **CFD simulation of combustible solid waste pyrolysis in a fluidized bed reactor**, Powder Technology, 362 (2020), pp. 177-187.

[17] J.M. Encinara, J.F. González, **Pyrolysis of synthetic polymers and plastic wastes. Kinetic study**, Fuel Process. Technol., 89 (2008), pp. 678-686.

[18] J. Ceamanos, J.F. Mastral, A. Millera, M.E. Aldea, **Kinetics of pyrolysis of high density polyethylene. Comparison of isothermal and dynamic experiments**, J. Anal. Appl. Pyrolysis, 63 (2002), pp. 93-110.

[19] H. Bockhorn, A. Hornung, U. Hornung, D. Schawaller, **Kinetic study on the thermal degradation of polypropylene and polyethylene**, J. Anal. Appl. Pyrolysis, 48 (1999), pp. 93-109.

[20] Z. Gao, I. Amasaki, M. Nakada, **A thermogravimetric study on thermal degradation of polyethylene**, J. Anal. Appl. Pyrolysis, 67 (2003), pp. 1-9.

[21] S. Kim, D. Kavitha, T.U. Yu, J. Jung, J. Song, S. Lee, *et al.*, **Using isothermal kinetic results to estimate kinetic triplet of pyrolysis reaction of polypropylene**, J. Anal. Appl. Pyrolysis, 81 (2008), pp. 100-105.

[22] S. Kim, Y. Kim, **Using isothermal kinetic results to estimate the kinetic triplet of the pyrolysis of high density polyethylene**, J. Anal. Appl. Pyrolysis, 73 (2005), pp. 117-121.

[23] A. Aboulkas, K. El Harfi, A. El Bouadili, **Non-isothermal kinetic studies on co-processing of olive residue and polypropylene**, Energy Convers. Manage., 49 (2008), pp. 3666-3671.

[24] L. Zhou, T. Luo, Q. Huang, **Co-pyrolysis characteristics and kinetics of coal and plastic blends**, Energy Convers. Manage., 50 (2009), pp. 705-710.

[25] S. Madruga, N. Haruki, A. Horibe, **Experimental and numerical study of melting of the phase change material tetracosane**, International Communication in Heat and Mass Transfer, 98 (2018), pp. 163-170.

[26] R. E. Murray and D. Groulx, **Modelling Convection during Melting of a Phase Change Material**, COMSOL Conference Boston, (2011).

[27] F. Samara, D. Groulx, and P. H. Biwole, **Natural Convection Driven Melting of Phase Change Material: Comparison of Two Methods**, COMSOL Conference Boston, (2012).

[28] D. Salvi, D. Boldor, G.M. Aita, C.M. Sabliov, **COMSOL Multiphysics model for continuous flow microwave heating of liquids**, Journal of Food Engineering, 104 (2011), pp. 422-429.

[29] L. J. Yin, D. Z. Chen, H. Wang, X. B. Ma, G. M. Zhou, **Simulation of an innovative reactor for waste plastics pyrolysis**, Chemical Engineering Journal, 237 (2014), pp. 229-235.

[30] **Typical Engineering Properties of Polypropylene**, INEOS Olefins and Polymers USA.

[31] **Typical Engineering Properties of High Density Polyethylene**, INEOS Olefins and Polymers USA.

[32] J. F. Asassant, F. Pigeonneau, L. Sardo, M. Vincent, **Flow analysis of the polymer spreading during extrusion additive manufacturing**, Additive Manufacturing, 29 (2019), pp. 100794.

[33] H.L. Friedman, **Kinetics of thermal degradation of char-forming plastic from thermogravimetry. Application to a phenolic plastic**, J. Polym. Sci., 6 (1964), pp. 183-195.

[34] J.M. Criado, **Kinetic analysis of DTG data from master curve**, Thermochim. Acta., 24 (1978), pp. 186-189.

[35] S. Vyazovkin, A.K. Burnham, J.M. Criado, L.A. Pérez-Maqueda, C. Popescud, N. Sbirrazzuolie, **Kinetics Committee recommendations for performing kinetic computations on thermal analysis data**, Thermochim. Acta., 520 (2011), pp. 1-19.

[36] **Heat Transfer Module User's Guide**, COMSOL Multiphysics.

[37] FRANK P. INCROPERA, **Fundamentals of Heat and Mass Transfer**, SIXTH EDITION, College of Engineering University of Notre Dame (2007).

[38] Dawei Li, Liwei Zhou, Xuan Wang, Lijuan He, and Xiong Yang, **Effect of Crystallinity of Polyethylene with Different Densities on Breakdown Strength and Conductance Property**, Materials (Basel), (2019).

[39] Analytical Answers, Differential Scanning Calorimetry (DSC), (2016).

[40] Hitachi High-Tech, DSC Measurement of Polyethylene, (1986).

[41] Roger L. Blaine, **Determination of Polymer Crystallinity by DSC**, TA Instruments.

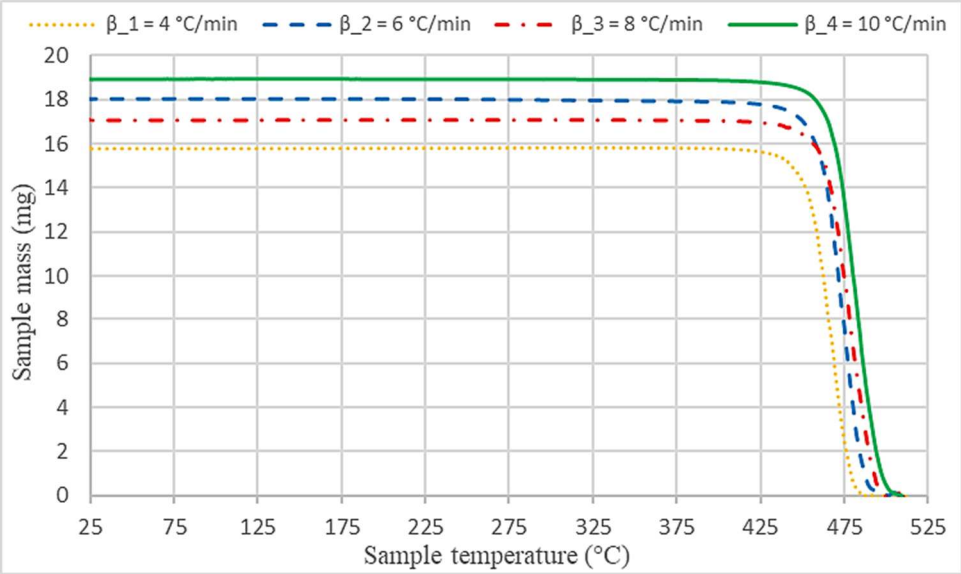

Fig. 1. Mass versus temperature for HDPE pyrolysis at different heating rates.

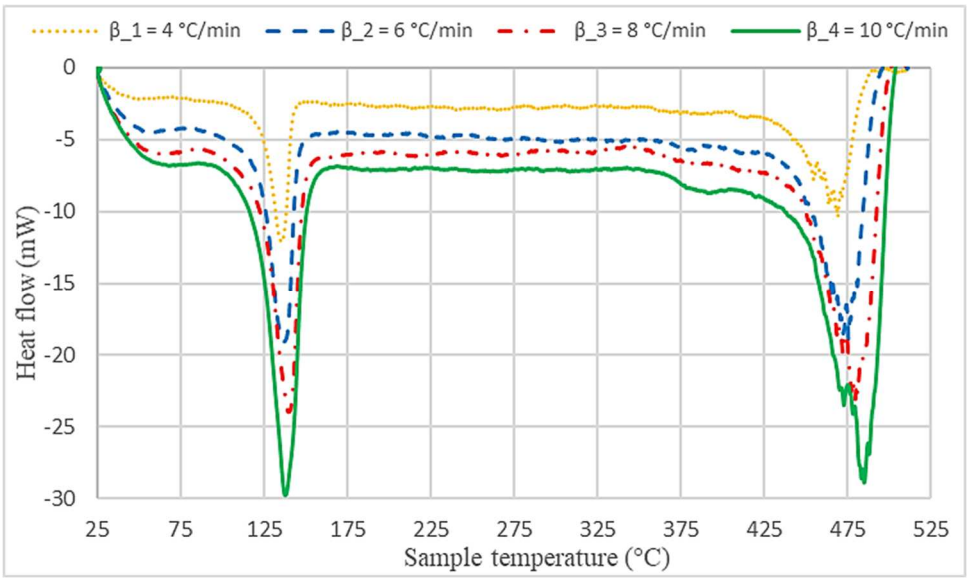

Fig. 2. Heat flow versus temperature for HDPE melting and pyrolysis at different heating rates.

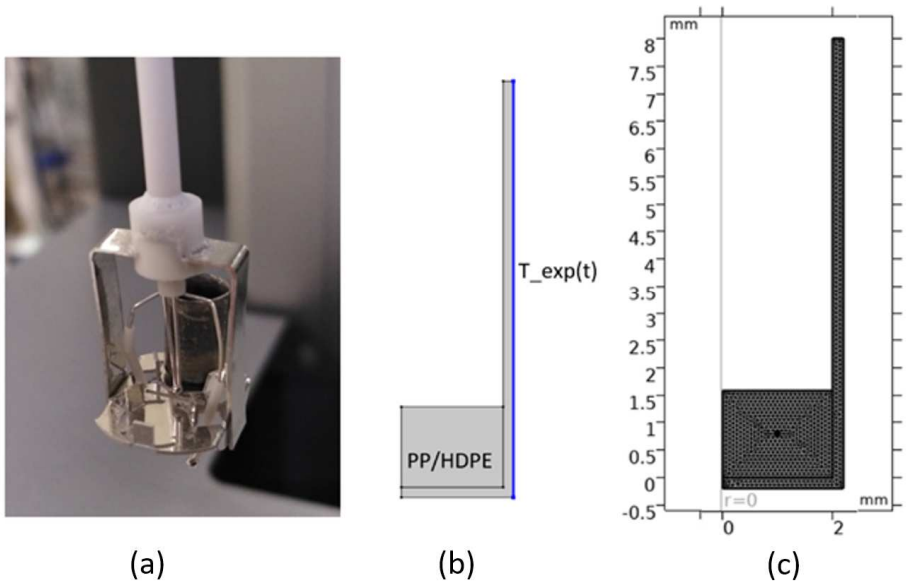

Fig. 3: (a) Real sample crucible image of the DSC/TGA analyzer, (b) 2D-axisymetric crucible model, and (c) Mesh display.

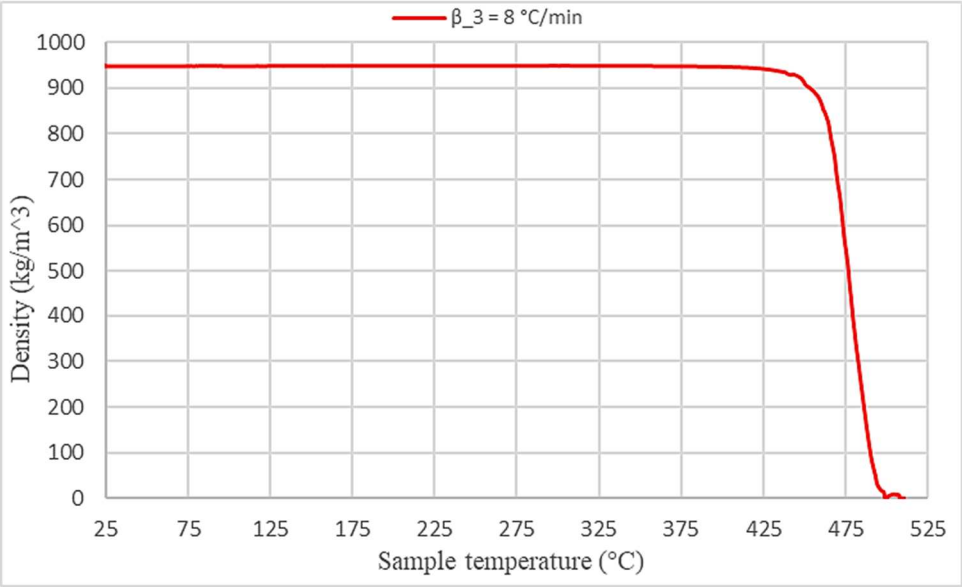

Fig. 4. Density versus temperature for HDPE used to model the mass loss for 8 °C/min heating rate.

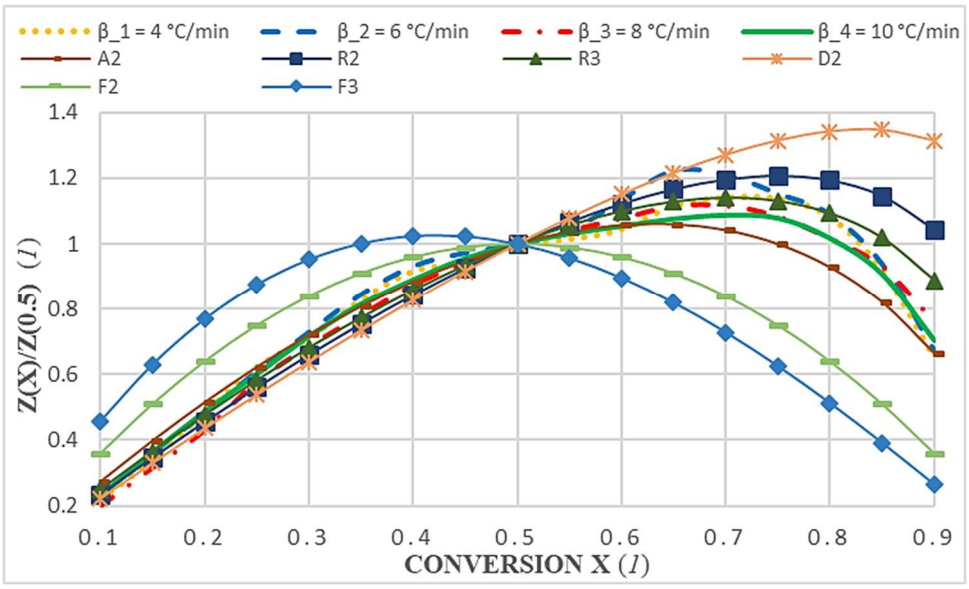

Fig. 5. Theoretical master plots for different reaction models compared with the experimental data for PP pyrolysis at different heating rates.

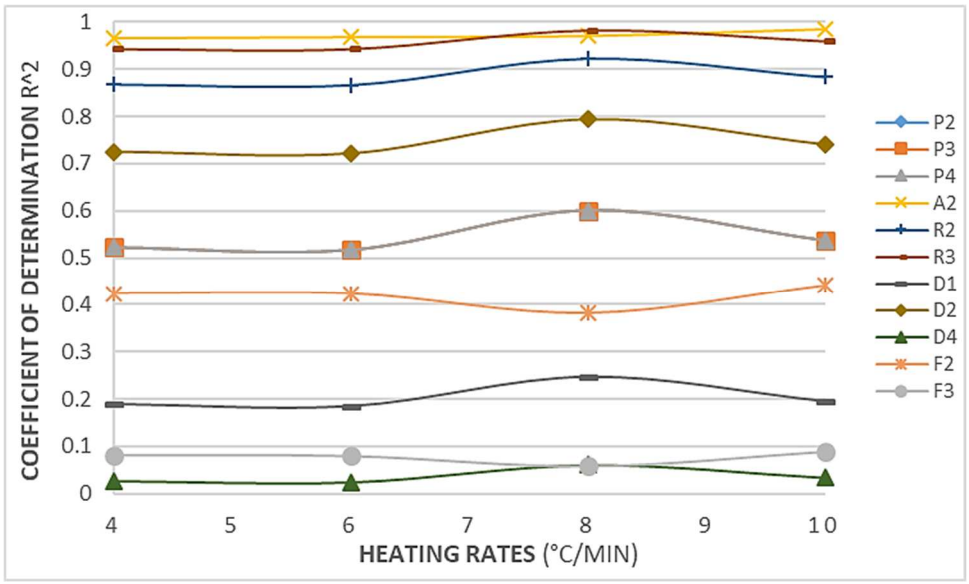

Fig. 6. Coefficient of determination R^2 versus heating rates, for PP pyrolysis, for different reaction models.

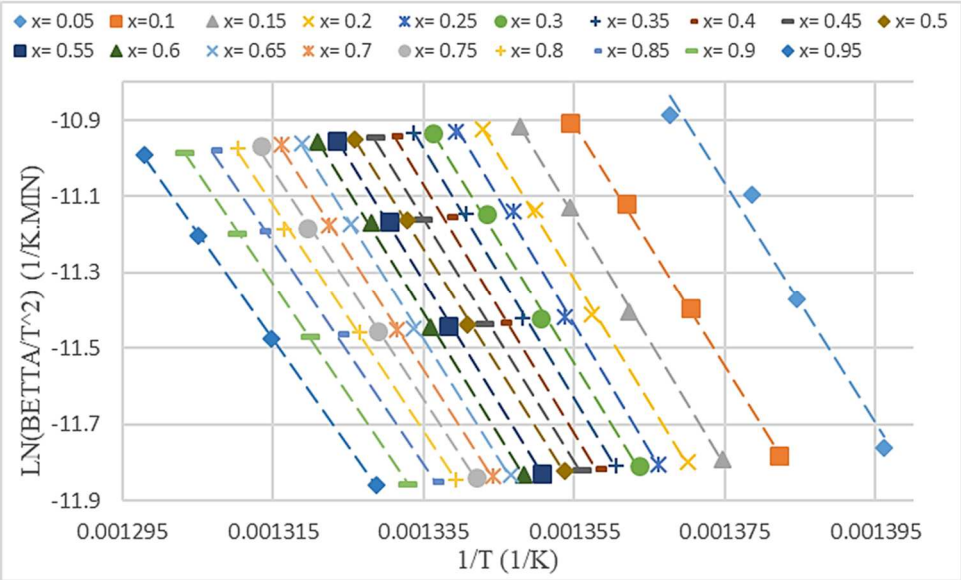

Fig. 7. Plotting $\ln(\beta/T^2)$ w.r.t. $1/T$, for HDPE pyrolysis, at each conversion for the heating rates (4, 6, 8, 10 °C/min) according to KAS method.

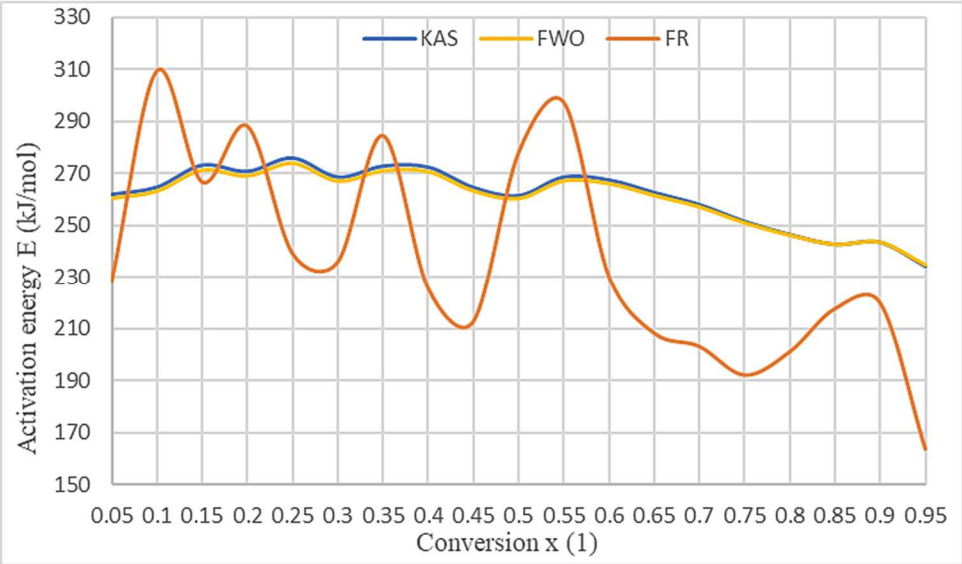

Fig. 8. Activation energy versus conversion for HDPE pyrolysis according three isoconversional methods; FR, KAS, and FWO.

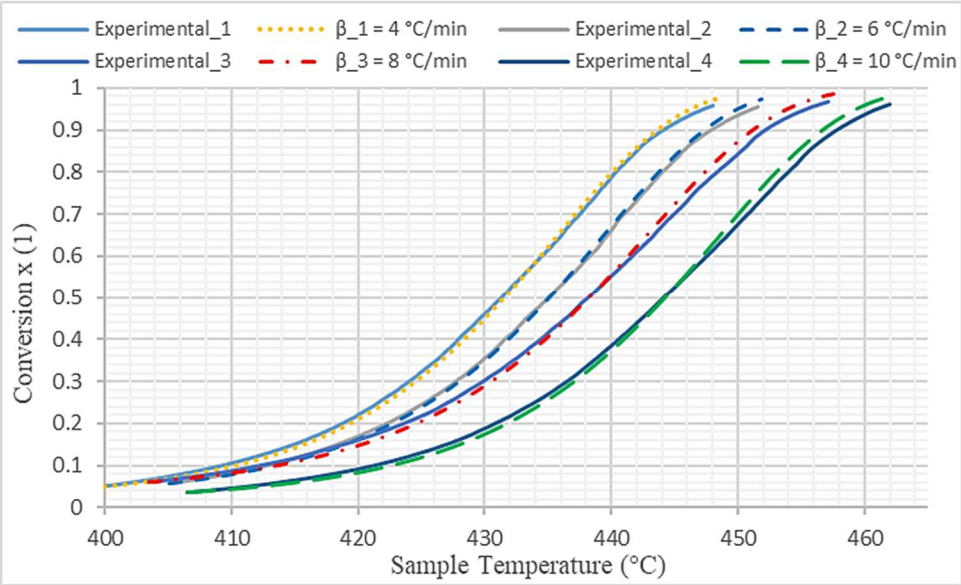

Fig. 9. Theoretical and experimental conversions for PP pyrolysis for four heating rates (4, 6, 8, and 10 °C/min), according to kinetic parameters (E = 220 (kJ/mol), f(x) is A2, and A = 4.15E+15 (1/min)).

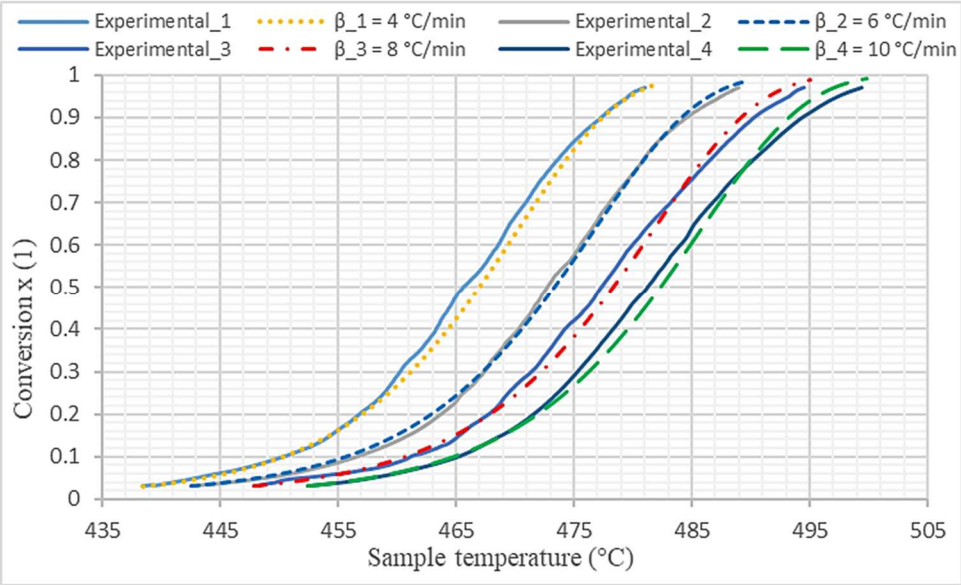

Fig. 10. Theoretical and experimental conversions for HDPE pyrolysis for four heating rates (4, 6, 8, and 10 °C/min), according to kinetic parameters (E = 264 (kJ/mol), f(x) is A2, and A = 8.3E+17 (1/min)).

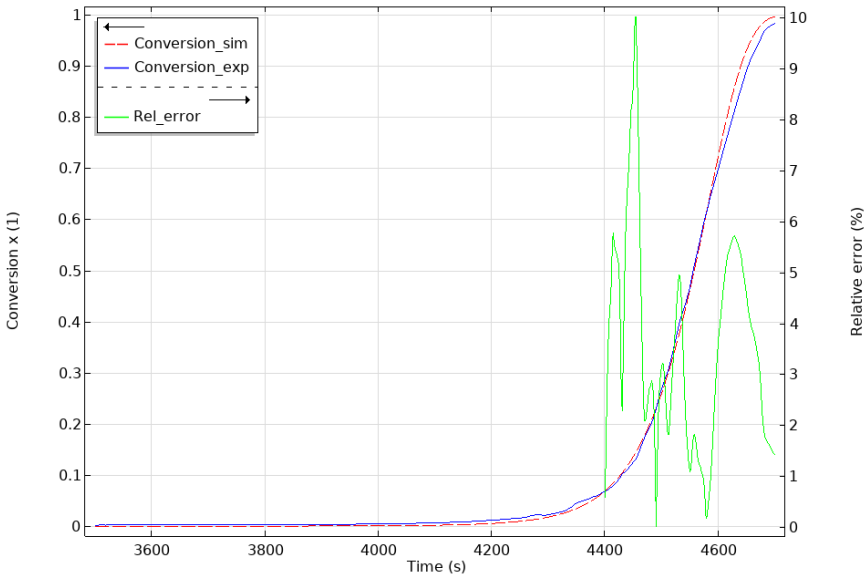

Fig. 11. Simulated and experimental conversion results for HDPE pyrolysis inside TGA-DSC, heating rate β_3= 8 °C/min.

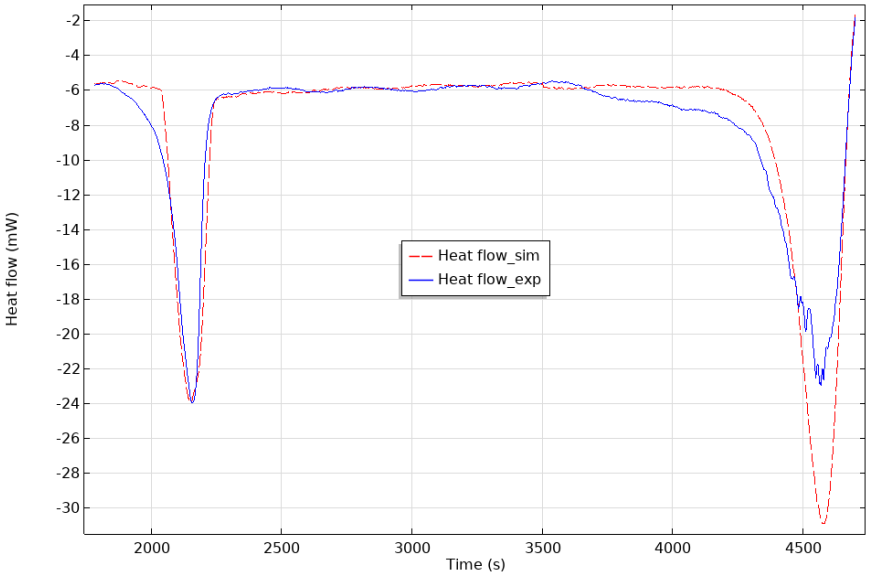

Fig. 12. Simulated and experimental heat flow results for HDPE pyrolysis inside TGA-DSC, heating rate β_3= 8 °C/min.

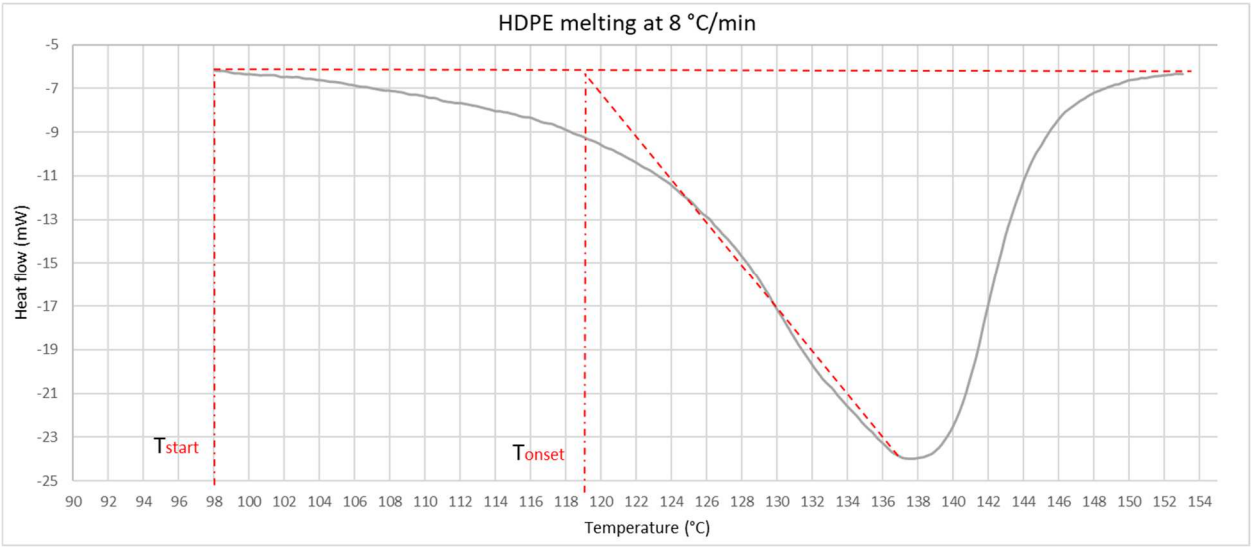

Fig. 13. Experimental heat flow results for HDPE melting inside TGA-DSC, heating rate β_3= 8 °C/min

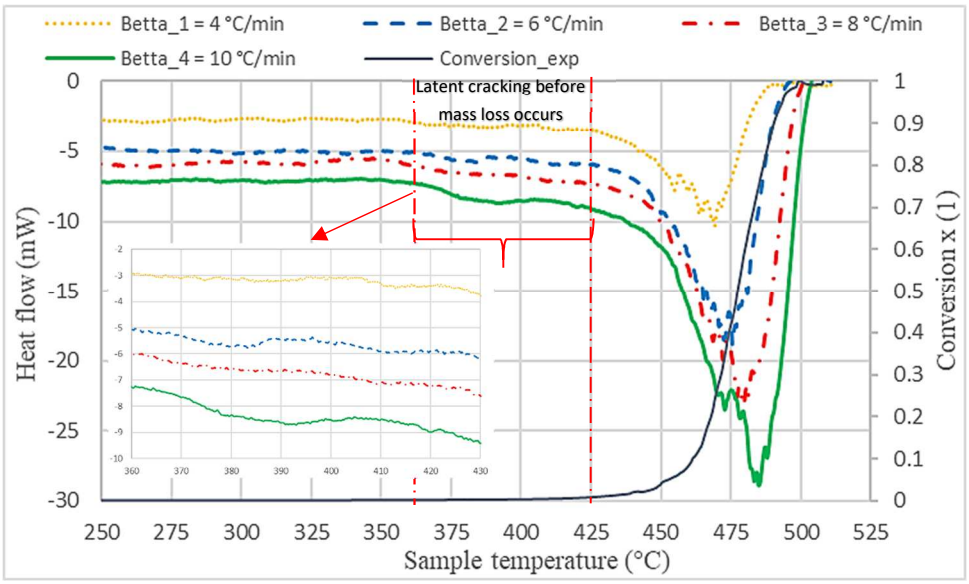

Fig. 14. Heat flow for HDPE pyrolysis, at different heating rates, illustrating the latent cracking phenomena before the mass loss cracking.

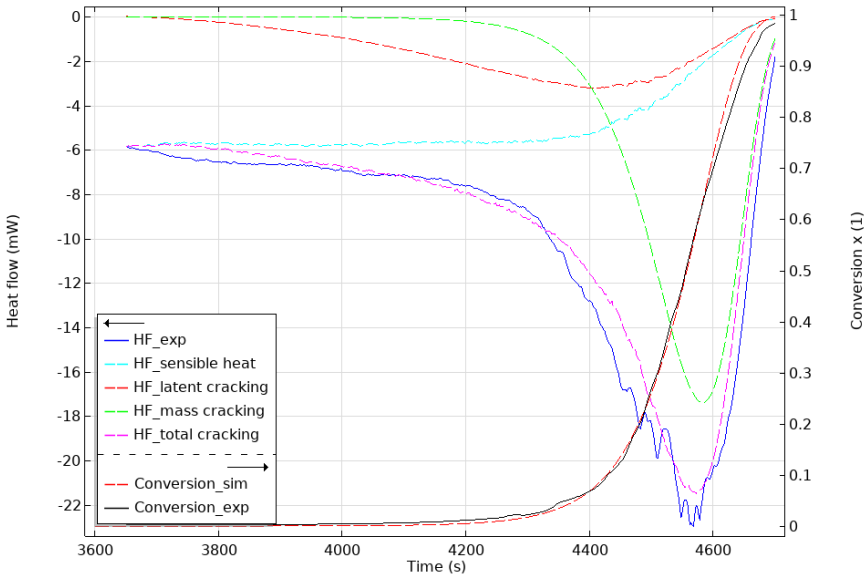

Fig. 15. Heat flow comparison for HDPE pyrolysis at 8 °C/min inside TGA-DSC according to the new enhanced model, latent cracking modelling.

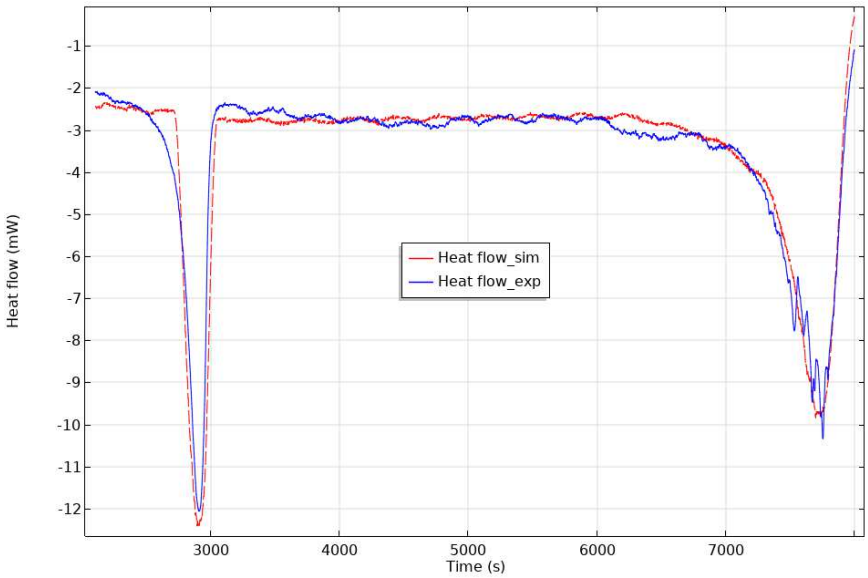

Fig. 16. Simulated and experimental results for HDPE pyrolysis at heating rate β_1= 4 °C/min.

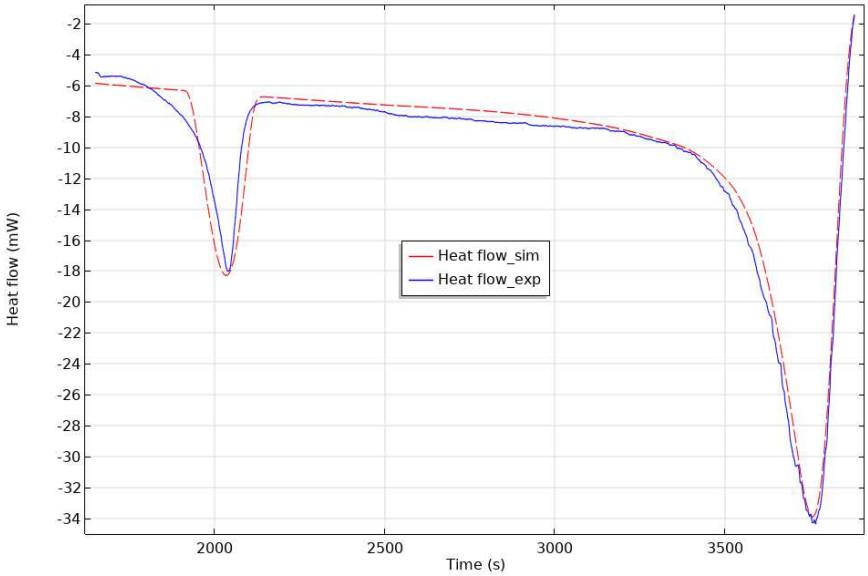

Fig. 17. Simulated and experimental results for PP pyrolysis at heating rate β_4= 10 °C/min.

Table 1
Peak temperatures and enthalpies, melting and cracking, for PP and HDPE at different heating rates.

	Peak temperature (°C)				Enthalpy (kJ/kg)			
	Melting		**Cracking**		**Melting**		**Cracking**	
Heating rate (°C/min)	**PP**	**HDPE**	**PP**	**HDPE**	**PP**	**HDPE**	**PP**	**HDPE**
4	153	135	431	467	59	117	415	295
6	154	137	437	475	62	123	423	320
8	155.5	138.5	440	479	66	127	435	334
10	157.5	140	444	483	69	130	445	345

Table 2
Thermo-physical properties for different materials within temperature range of 25 - 300 °C.

Materials	Thermal conductivity **k** (*W/K.m*)	Specific heat capacity $\mathbf{C_p}$ (*J/kg.K*)	Density $\boldsymbol{\rho}$ (kg/m^3)
PP	0.1 – 0.12	1800 – 2500	900
HDPE	0.42 – 0.45	1800 – 2500	950
Aluminum crucible	35	880	3900

Table 3
Reaction model for the most common reaction mechanism.

Mechanism	$f(x)$	$g(x)$
First-order (F1)	$(1-x)$	$-\ln(1-x)$
Second-order (F2)	$(1-x)^2$	$(1-x)^{-1}-1$
Third-order (F3)	$(1-x)^3$	$[(1-x)^{-2}-1]/2$
Power law (P2)	$2x^{1/2}$	$x^{1/2}$
Power law (P3)	$3x^{2/3}$	$x^{1/3}$
Power law (P4)	$4x^{3/4}$	$x^{1/4}$
One-dimensional diffusion (D1)	$1/2(x)$	x^2
Two-dimensional diffusion (D2)	$[-\ln(1-x)]^{-1}$	$[(1-x)\ln(1-x)]+x$
Three-dimensional diffusion (D3)	$3(1-x)^{2/3}/\left[2\left(1-(1-x)^{1/3}\right)\right]$	$\left[1-(1-x)^{1/3}\right]^2$
Ginstling-Brounshtein (D4)	$3/2\left[(1-x)^{-1/3}-1\right]$	$1-(2x/3)-(1-x)^{2/3}$
Contracting cylinder (R2)	$2(1-x)^{1/2}$	$\left[1-(1-x)^{1/2}\right]$
Contracting sphere (R3)	$3(1-x)^{2/3}$	$\left[1-(1-x)^{1/3}\right]$
Avarami-Erofe'ye (A2)	$2(1-x)[-\ln(1-x)]^{1/2}$	$[-\ln(1-x)]^{1/2}$
Avarami-Erofe'ye (A3)	$3(1-x)[-\ln(1-x)]^{2/3}$	$[-\ln(1-x)]^{1/3}$
Avarami-Erofe'ye (A4)	$4(1-x)[-\ln(1-x)]^{3/4}$	$[-\ln(1-x)]^{1/4}$

Table 4
Deduced average kinetic parameters for PP and HDPE pyrolysis

	PP			**HDPE**	
		A (1/min)			**A** (1/min)
Method	**E** (kJ/mol)	A2	R3	**E** (kJ/mol)	A2
FR	202	8.78×10^{14}	3.27×10^{14}	238	1.87×10^{19}
KAS & FWO	220	4.15×10^{15}	1.27×10^{15}	264	8.3×10^{17}

Table 5
Average kinetic parameters for PP and HDPE pyrolysis

	PP		**HDPE**	
		A (1/min)		**A** (1/min)
Method	**E** (kJ/mol)	A2	**E** (kJ/mol)	A2
KAS & FWO	220	4.15×10^{15}	264	8.3×10^{17}

Table 6
Mass loss enthalpies and deduced latent cracking enthalpies.

	ΔH_{mc}	ΔH_{lc}	ΔH_{c}
PP	280	130	424
HDPE	200	100	323